Journal of Solid State Chemistry 198 (2013) 496–505

Contents lists available at SciVerse ScienceDirect

Journal of Solid State Chemistry

journal homepage: www.elsevier.com/locate/jssc

pH control of the structure, composition, and catalytic activity of sulfated zirconia

Vladimir K. Ivanov [a,b], Alexander Ye. Baranchikov [a,c,*], Gennady P. Kopitsa [d], Sergey A. Lermontov [e], Lyudmila L. Yurkova [e], Nadezhda N. Gubanova [a,d], Olga S. Ivanova [a], Anatoly S. Lermontov [a], Marina N. Rumyantseva [c], Larisa P. Vasilyeva [f], Melissa Sharp [g], P. Klaus Pranzas [g], Yuri D. Tretyakov [b]

[a] Kurnakov Institute of General and Inorganic Chemistry of Russian Academy of Sciences, Leninsky ave., 31, Moscow 119991, Russian Federation
[b] Materials Science Department, Moscow State University, Moscow 119991, Russian Federation
[c] Department of Chemistry, Moscow State University, Moscow 119991, Russian Federation
[d] Petersburg Nuclear Physics Institute, Orlova Roscha, Gatchina 188300, Russian Federation
[e] Institute of Physiologically Active Compounds of the Russian Academy of Sciences, Chernogolovka 142432, Russian Federation
[f] Institute of Problems of Chemical Physics, Russian Academy of Sciences, Chernogolovka 142432, Russian Federation
[g] GKSS Forschungszentrum, Geesthacht 21502, Germany

ARTICLE INFO

Article history:
Received 30 July 2012
Received in revised form
12 October 2012
Accepted 18 November 2012
Available online 30 November 2012

Keywords:
Sulfated zirconia
Small-angle neutron scattering
Mesostructure
Fractal properties

ABSTRACT

We report a detailed study of structural and chemical transformations of amorphous hydrous zirconia into sulfated zirconia-based superacid catalysts. Precipitation pH is shown to be the key factor governing structure, composition and properties of amorphous sulfated zirconia gels and nanocrystalline sulfated zirconia. Increase in precipitation pH leads to substantial increase of surface fractal dimension (up to ~2.7) of amorphous sulfated zirconia gels, and consequently to increase in specific surface area (up to ~80 m^2/g) and simultaneously to decrease in sulfate content and total acidity of zirconia catalysts. Complete conversion of hexene-1 over as synthesized sulfated zirconia catalysts was observed even under ambient conditions.

1. Introduction

Superacids including sulfated titania, zirconia, and stannia are among the most promising heterogeneous catalysts [1]. Their acidity is much higher even than that of concentrated H_2SO_4, with their surface sulfate groups acting as Lewis and Brønsted sites [2]. The main advantages of solid superacid oxide catalysts include high stability at elevated temperatures, resistance to deactivation, and easy regeneration. The SO_4/ZrO_2 is the most comprehensively studied system because its acidity is one of the highest among the sulfated oxides [2,3]. The Hammett acidity functions H_0 for SO_4/ZrO_2 and SO_4/SnO_2 fall within the range from −16 to −18; SO_4/TiO_2 has a slightly lower value of −14.6 [4]. The above indicated values can vary because of the lack of common procedures for analysis of the properties of sulfated oxides [5]. Reproducibility of synthetic procedures used to prepare sulfated oxides is still also rather poor [1].

The most common route to prepare fine zirconia powders includes precipitation of amorphous hydrous zirconia from aqueous or alcoholic solutions and its further treatment (e.g., drying, milling and annealing). Typical procedure for a sulfated zirconia catalyst synthesis includes impregnation of thus obtained amorphous $ZrO_2 \cdot xH_2O$ or crystalline ZrO_2 with sulfate-containing compounds (e.g., sulfuric acid, ammonium persulfate) [3,6]. Thus characteristics of nanocrystalline zirconia-based materials should depend on the composition and structure of intermediate amorphous phases formed during hydrolysis of Zr(IV) compounds. Recently [7] we have demonstrated that variation in the precipitation pH indeed considerably changes the mesostructure, fractal dimension and specific surface area of hydrous zirconia and hafnia gels. Thermal decomposition of these gels actually gives rise to ZrO_2 and HfO_2 nanopowders having considerably different particle sizes and specific surface areas.

In this paper, we aimed at establishing the probable interrelation between the composition and the mesostructure of amorphous zirconia gels and phase composition, structure and catalytic activity of sulfated zirconia prepared thereof. To synthesize sulfated zirconia we have used a simple procedure which includes only two steps: one-pot precipitation of sulfated hydrous

* Corresponding author at: Kurnakov Institute of General and Inorganic Chemistry of Russian Academy of Sciences, Leninsky ave., 31, Moscow 119991, Russian Federation. Fax: +7 495 9541279.
E-mail address: a.baranchikov@yandex.ru (A.Ye. Baranchikov).

0022-4596/$ - see front matter © 2012 Published by Elsevier Inc.
http://dx.doi.org/10.1016/j.jssc.2012.11.022

zirconia gels at various pHs and their further annealing. We hope that such an approach would favour reproducibility of structure and composition of sulfated zirconia catalysts and thus their catalytic properties.

2. Experimental

2.1. Synthesis of samples

All starting materials used in the experiments were of analytical grade. Zirconium oxynitrate hydrate ($ZrO(NO_3)_2 \cdot xH_2O$, 99% Aldrich) was dissolved in distilled water and then ammonium sulfate (99%, Chimmed, Russia) was added so that the final concentrations of $ZrO(NO_3)_2$ and $(NH_4)_2SO_4$ were 0.25 M and 1.0 M, respectively. The resulting solution was kept overnight and then filtered. To obtain hydrous sulfated zirconia, aqueous ammonia (2.7 M, 99%, Chimmed, Russia) was added dropwise to the starting zirconium-containing solution under vigorous stirring until the desired pH value was reached (3.98, 6.98 or 8.98). pH measurements were made using Crison GLP-22 pH-meter. Obtained suspensions were additionally stirred for 30 min in mother liquor while pH value was carefully adjusted with aqueous ammonia. The resultant white precipitates were washed four times by redispersion in distilled water followed by centrifugation (8000 min^{-1}). All the samples were further dried in an oven under air flow at 50 °C overnight and carefully grounded in an agate mortar. Hereafter the as-synthesized sulfated hydrous zirconia xerogels precipitated at pH 3.98, 6.98 or 8.98 are named Z-4S, Z-7S and Z-9S, respectively.

Thermal decomposition of the xerogels was conducted in a muffle furnace in air at 500 °C, 550 °C, 600 °C and 700 °C for 5 h. Heating rate was 10 °C/min. After the annealing samples were cooled down to ambient temperature within the furnace. Resulting sulfated zirconia powders are named hereafter Z-4S–*T*, Z-7S–*T*, Z-9S–*T* (here *T* is a temperature of thermal treatment—500 °C, 550 °C, 600 °C or 700 °C), respectively.

Throughout this paper the characteristics of sulfated zirconia are compared with the properties of zirconia samples synthesized using the same procedure but without addition of ammonium sulfate to the starting solution [7].

2.2. Methods of analysis

X-ray powder diffractograms (XRD) were obtained using Rigaku D/MAX 2500 diffractometer (Cu K_α radiation) over a 2θ range of 10–85° with an increment 0.02°/step at the rate 2 °/min. Particle size was estimated using Scherrer equation

$$D = \frac{K\,\lambda}{[\beta(2\theta) - s]\cos\theta_0} \quad (1)$$

Here, θ_0 is the peak position, λ is the Cu K_α radiation wavelength (0.154,056 nm), $\beta_{hkl}(2\theta)$ is the FWHM of a corresponding peak, s is the instrumental broadening (is equal to 0.1°). The value of K (shape factor) was set equal to 1. The β value was determined by subtraction of background followed by fitting profiles of (1 1 1) and (1 $\bar{1}$ 1) reflections of monoclinic zirconia and (1 1 1) reflection of tetragonal zirconia to the Voigt pseudo-functions. Volume fractions of monoclinic (m-ZrO_2) and tetragonal (t-ZrO_2) phases in zirconia samples were estimated using relations proposed by Toraya et al. [8].

Thermal analysis (TGA/DTA) of the samples was performed in air using Pyris Diamond thermoanalyzer (Perkin–Elmer) in the temperature range 20–1100 °C (heating rate 10 °C/min). Chemical composition of gases evolved during thermal decomposition under argon flow was established by means of Netzsch STA 449 F1 Jupiter thermal analyzer equipped with mass-spectrometer (heating rate 5 °C/min).

Transmission electron microscopy images were taken using Leo 912 AB Omega electron microscope operating at 100 kV. Microstructure of the samples was also studied using Carl Zeiss NVision 40 scanning electron microscope (micrographs were obtained at 1 kV acceleration voltage) equipped with Oxford Instruments X-MAX energy-dispersive X-ray (EDX) analyzer operating at 30 kV acceleration voltage. The samples were not specially prepared (e.g., coated with conducting material) for TEM and SEM measurements. Before EDX analysis samples were coated with ~5 nm Au/Pd.

Low temperature nitrogen adsorption measurements were conducted using ATX-6 analyzer (Katakon, Russia) at −196 °C. Before measurements the samples were outgased at 200 °C for 30 min under dry helium flow. Determination of the surface area was carried out by 8-point Brunauer–Emmett–Teller (BET) method.

To study the influence of precipitation conditions on the mesostructure of amorphous zirconia xerogels a small angle neutron scattering (SANS) technique was used. SANS measurements were performed on SANS-2 setup (FRG-1 neutron reactor, GKSS Research Centre, Geesthacht, Germany). The experiments were performed at neutron wavelength $\lambda = 5.8$ Å with $\Delta\lambda/\lambda = 10\%$ and for four sample-detector distances $SD = 1$ m, 3 m, 7 m, and 20.7 m, which allowed to perform the measurements of the neutron scattering intensity for momentum transfers in the range $2.5 \times 10^{-3} < q < 2.6 \times 10^{-1}$ $Å^{-1}$. The scattered neutrons were detected by a two-dimensional position-sensitive ^{3}He detector.

The samples of amorphous xerogels of sulfated hydrous ZrO_2 were placed in a 1 mm thick quartz cells. Apparent density ρ_H of each sample was calculated as a weight of a powder divided by its volume. The initial spectra for each q range were corrected using the standard procedure [9] taking into account the scattering from the setup equipment and cell, as well as background from incoherent scattering of neutrons on hydrogen atoms which are present in samples in the form of physically and chemically bounded water. Resulting 2D isotropic spectra were averaged azimuthally and their absolute values were determined by normalizing to the incoherent scattering cross section from vanadium with inclusion of the detector efficiency and apparent density (ρ_H) for each sample. All measurements were done at room temperature.

The SANS intensity analyzed hereafter was defined as

$$I_S(q) = I(q) - T \times I_0(q), \quad (2)$$

where $I(q)$ and $I_0(q)$ are the momentum-transfer distributions of scattered neutrons behind the sample and beam without the sample, respectively. $T = I/I_0 = \exp(-\Sigma \times L)$ is the transmission coefficient of the neutrons passing through the sample, where $\Sigma = \sigma_s + \sigma_a$ is the integral scattering cross section which includes nuclear scattering σ_s and absorption σ_a, and L is the sample thickness. The setup resolution function was approximated by a Gaussian and was calculated separately for each SD distance with the use of the standard procedure [10].

Adsorption of NH_3 for temperature-programmed desorption experiments (NH_3-TPD) was performed using Chemisorb 2750 (Micromeritics) in NH_3:N_2 = 5:95 (v/v) gas mixture. Before the experiments, the samples were pretreated for 1 h at 300 °C under helium flow (30 ml/min), then for 1 h at 300 °C under O_2:N_2 = 20:80 (v/v) gas mixture (30 ml/min) and finally for 30 min at room temperature under O_2:N_2 = 20:80 (v/v) gas mixture (30 ml/min). NH_3-TPD was carried out under helium flow after purging the sample at 50 °C for 20 min to decrease the amount of physisorbed ammonia.

Studies of catalytic activity of Z-4S-600, Z-7S-600, Z-9S-600 samples in hexene-1 oligomerization were performed as follows.

Before a reaction each sample was heated in air at 600 °C for 2 h and then cooled in dry atmosphere. A 1 g portion of catalyst and 5 ml (3.4 g) of hexene-1 were placed into a thermostated glass flask and kept at constant temperature in 20–60 °C range under vigorous stirring. Samples of the reaction mixtures (0.2 ml) were taken for ^{1}H–NMR and GC–MS analyses. ^{1}H NMR spectra were recorded using a Bruker DPX-200 spectrometer in $CDCl_3$. NMR spectra gave a possibility to monitor a vinyl group protons disappearance. Gas chromatography (GC) and GC–MS were performed using a LHM-2000 chromatograph (3% Dexsil 300—Chrom W–AW column) and Perkin–Elmer Clarus 500 (SE-30 column) spectrometer, respectively. These data were used to determine oligomers content in reaction mixtures.

3. Results and discussion

Fig. 1 shows the experimental curves of differential neutron cross section $d\Sigma(q)/d\Omega$ for amorphous sulfated zirconia xerogels precipitated at different pHs. According to these data, increase in the precipitation pH from 3.98 to 8.98 leads to notable (approximately two orders of magnitude) increase in SANS intensity as well as to changes in scattering pattern. This clearly indicates that the nuclear density homogeneity of xerogels in the range 10–1000 Å is decreased with the increase in the precipitation pH.

Sample synthesized in acidic media (Z-4S) shows two various q ranges which significantly differ by the behavior of the SANS cross section $d\Sigma(q)/d\Omega$. For low values $q < q_{c1}$ (where $q_{c1} \approx 0.06$ Å^{-1} is the transition point between one scattering regime and another), the scattering cross-section $d\Sigma(q)/d\Omega$ satisfies the power law q^{-n}. Such a power-law dependence is typical for systems with a wide size distribution ($R_{max} \gg R_{min}$) if the condition

$$R_{max}^{-1} << q << R_{min}^{-1} \tag{3}$$

is satisfied. In addition, the power scattering law means that inhomogeneities making the dominant contribution to scattering are sufficiently large ($q_{min} \cdot R \gg 1$). Bale and Schmidt [11] proposed a more exact criterion for determination of a certain characteristic size of inhomogeneities, $q_{min} \cdot R \approx 3.5$. In our case, $q_{min} = 2.5 \cdot 10^{-3}$ Å^{-1} and consequently the characteristic size of the inhomogeneities is $R \approx 1250$ Å.

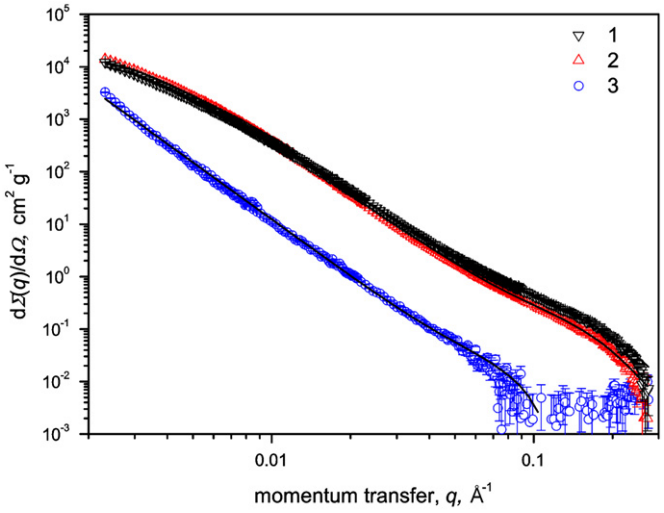

Fig. 1. SANS differential cross-section $d\Sigma(q)/d\Omega$ for amorphous sulfated zirconia, precipitated at pH=8.98 (1), 6.98 (2), and 3.98 (3) versus momentum transfer q. Continuous lines represent results of experimental data fitting.

The exponent n value for the Z-4S sample found from the slope of the straight-line section of the experimental $d\Sigma(q)/d\Omega$ plotted in log–log scale is equal to 3.68. Thus scattering from the sample occured on the fractal surface with the dimension $2 \le D_S = 6 - n = 2.32 < 3$. In the $q > q_{c1}$ region, the scattering curve exhibits a shoulder indicating the presence of small inhomogeneities with the effective gyration radius $r_g = 33 \pm 2$ Å.

Thus, the Z-4S xerogel contains two types of scattering inhomogeneities with strongly different characteristic sizes which correspond to relatively large aggregates with a fractal surface and small monomer particles.

The absence of the Guinier region on the scattering curve for low q-values means that the gyration radius r_g or, for the fractal systems, the upper self-similarity boundary is larger than the maximum size R_{max} of the inhomogeneities that can be detected in the experiment with a given resolution. In turn, the lower self-similarity boundary is likely to be determined by the size r_c of small inhomogeneities, which usually lies in the range from $2r_g$ to $3r_g$ (approximately $2.6r_g$ for spherical particles) [12].

SANS cross-section for the samples Z-7S and Z-9S as distinguished from Z-4S has higher intensity and possesses an extra region in the range of small q-values ($q < q_{c2} \approx 0.005$ Å^{-1}), where the deviation of $d\Sigma(q)/d\Omega$ from power-law q^{-n} is observed. This deviation is due to the transition to Guinier regime, where cross-section is governed by relatively large scattering inhomogeneities with characteristic size r_c (aggregates). As for the region $q > q_{c1}$, the scattering curves also exhibit a shoulder due to the scattering on small inhomogeneities, while this shoulder appears at larger q-values compared to the spectrum of Z-4S sample. This indicates that precipitation of sulfated hydrous zirconia at higher pH leads to decrease in the primary particles size r_c. Moreover, despite we cannot estimate the upper limit of self-similarity range for all the samples, the widest self-similarity range can be ascribed to the xerogel synthesized at the lowest pH. Values of n parameter as calculated from linear slopes of spectra for samples Z-7S and Z-9S are equal to 3.43 and 3.17, respectively.

SANS from sulfated hydrous zirconia xerogels is in a good accordance with our previously reported data [7,13] indicating that scattering from non-sulfated zirconia precipitated at pH > 6 can be described within the model of porous structure with fractal surface.

In view of this circumstance, to analyze scattering from Z-7S and Z-9S amorphous xerogels over the entire q range, we used the expression [13,14]:

$$\frac{d\Sigma(q)}{d\Omega} = A_1 \times \exp\left(-\frac{q^2 R_g^2}{3}\right) + \frac{A_2(D_S)}{(\hat{q})^n} + A_3 \times \exp\left(-\frac{q^2 r_g^2}{3}\right) \tag{4}$$

Here,

$$\hat{q} = q/[\mathrm{erf}\left(q \times R_g/6^{1/2}\right)]^3 \tag{5}$$

is the momentum q transferred, normalized to an error function erf(x). Such a procedure allows the cross-section of scattering $d\Sigma(q)/d\Omega$ to be described correctly in the intermediate region between $q \cdot R_0 < 1$ (Guinier approximation) and $q \cdot R_0 \gg > > 1$ (q^{-n} asymptotics), where scattering from both surfaces and aggregates of characteristic size R_0 contributes [14]. The values of A_1 and A_3 are directly proportional to the number and the volume of inhomogeneities (aggregates and monomers, respectively) as well as to the density of their neutron scattering amplitudes [15]. Amplitude $A_2(D_S)$ depends on the fractal dimension of the system [11] as

$$A_2(D_S) = \pi \rho^2 \Gamma(5 - D_S) \sin[(D_S - 1)(\pi/2)] N_0 \tag{6}$$

where Γ is the gamma function, and ρ for a compound containing several elements is defined as

$$\rho = \sum_i b_i N_i \frac{\rho_h N_A}{M}. \quad (7)$$

Here, N_A is the Avogadro constant, M is the molar mass, b_i is the scattering length for the ith element in the compound, N_i is the number of atoms of this element, and ρ_H is the solid-phase density. The constant N_0 is related to the specific surface of the surface fractal as $S_0 = N_0 \cdot r^{2-Ds}$, where r^{2-Ds} is determined by the length of the yardstick. For smooth surfaces, $D_S = 2$ and $N_0 = S_0$.

Taking into account that for the Z-4S sample no deviation of scattering spectrum from power-law dependence in small q range was observed, expression (4) was simplified to:

$$\frac{d\Sigma(q)}{d\Omega} = \frac{A_2(D_S)}{q^n} + A_3 \times \exp\left(-\frac{q^2 r_g^2}{3}\right) \quad (8)$$

To obtain the final results, expressions (4, 8) were convolved with the setup resolution function. The experimental curves of the differential cross section $d\Sigma(q)/d\Omega$ versus q were processed by the least mean squares method over the entire q range under investigation. The results of this analysis are given in Table 1.

These data evidently show that both surface fractal dimension and $A_2(D_S)$ values increase with the increase in the precipitation pH. The value of D_S for the sample Z-4S is the lowest, i.e., in this case monomer particles form fractal aggregates with the smoothest surface. Upon precipitation from neutral (pH=6.98) and alkaline (pH=8.98) media the values of surface fractal dimension are higher (2.6 and 2.8, respectively). In other words, increase in the precipitation pH results in notable changes in monomer aggregation behavior.

Formation of zirconia surface fractal aggregates and increase in their surface fractal dimension upon increase in pH can be explained using well known data on the mechanism of condensation of hydrous silica monomers [16]. Under acidic conditions condensation occurs mainly between silanol groups located at the ends of polymeric chains leading to the formation of linear polymers. Contrariwise, under basic conditions, the condensation reaction occurs preferentially between the ends and the interior of polymeric chains thus leading to formation of ramified aggregates with a higher fractal dimension. Such an approach explains the increase in the surface fractal dimension value of hydrous zirconia upon gradual increase in the precipitation pH from 4 to 9. These suppositions are also in agreement with well established Clearfield theory [17], which states that slow hydrolysis of zirconyl salts leads to formation of regular sheets consisting of tetrameric $[Zr_4(OH)_8]$ units, while fast hydrolysis (for instance, under basic conditions) promotes rapid polymerization occurring in many directions at once. The degree of polymerization increases with an increase in pH [18]. Such a mechanism of polymerization can be also the main reason of fractal formation in course of hydrous sulfated zirconia precipitation. In this case, further increase in pH will result in formation of hydrous zirconia samples possessing even higher surface fractal dimension.

Table 1
Parameters of mesostructure of amorphous sulfated zirconia according to SANS measurements.

	Zr-4S	Zr-7S	Zr-9S
$A_1 \times 10^{-6}$ (cm^2 g^{-1})	–	31,400 ± 2000	25,400 ± 2,000
R_0 (Å)	≥ 1,250	710 ± 70	690 ± 100
$A_2 \times 10^{-6}$ (cm^2 g^{-1})	0.8 ± 0.1	100 ± 25	210 ± 60
$D_S = 6 - n$	2.32 ± 0.09	2.57 ± 0.08	2.83 ± 0.08
$A_3 \times 10^{-1}$ (cm^2 g^{-1})	0.57 ± 0.05	4.08 ± 0.07	5.3 ± 0.08
r_g (Å)	33 ± 2	17.3 ± 0.8	15.1 ± 0.9

Fig. 2 shows SANS data for amorphous sulfated zirconia in comparison with our recent data for hydrous zirconia xerogels synthesized using precisely the same procedure excluding addition of ammonium sulfate to the starting solution [7]. Surface fractal dimension for both sulfated and non-sulfated zirconia xerogels increases with the increase in the precipitation pH (Fig. 2A). These data are in line with our earlier supposition that precipitation conditions influence strongly the mesostructure of zirconia xerogels and this effect is due to change in colloid particles aggregation mechanism upon change of acidity of the media and surface charge of colloid particles. On the other hand, D_S of sulfated zirconia is notably higher than D_S of non-sulfated zirconia within the whole pH range. This difference is probably due to the presence of doubly charged sulfate ions, which strongly adsorb onto the surface of colloid $ZrO_2 \cdot xH_2O$ particles, while nitrate ions have less sorption ability.

It is worth saying that reproducibility of structural parameters of hydrated zirconia gels as derived from small-angle neutron scattering data is very high. For instance, the fractal dimension of amorphous zirconia gels precipitated at given pH is always the same (namely, variation of D_S value is less then 0.02 from one experiment to another). In fact, from our point of view, such a reproducibility is a very amazing phenomenon. It clearly demonstrates that the "soft matter" is in fact not so "soft".

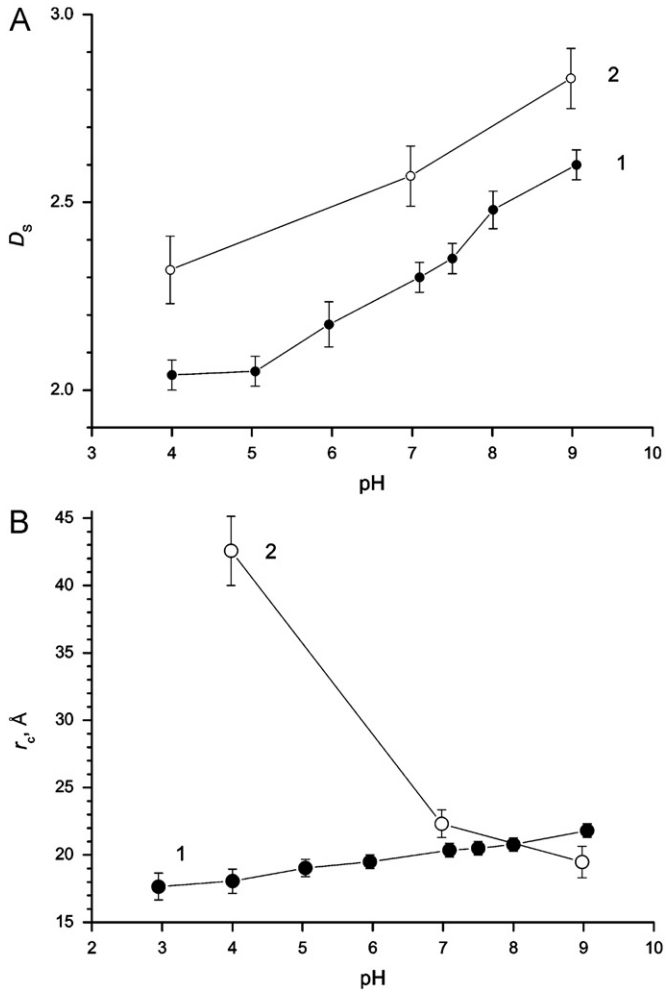

Fig. 2. Surface fractal dimension, D_S (A) and primary particle size, r_c (B) of amorphous zirconia xerogels versus precipitation pH. 1 – non-sulfated zirconia according to [7], 2 – sulfated zirconia synthesized in this work.

The rise of the precipitation pH from 3.98 to 8.98 leads to approximately twofold decrease in the characteristic size r_c (for spheres, $r_c=(5/3)^{1/2}r_g$) of primary sulfated $ZrO_2 \cdot xH_2O$ particles (from ~43 Å to ~20 Å, see Fig. 2B). For non-sulfated zirconia synthesized under the same conditions a slight increase in primary particle size (from ~18 to ~22 Å) is observed upon the rise of pH.

According to XRD data (see Fig. S1 in the Supporting Information) all the initial xerogels are completely amorphous giving two extremely broad peaks at ~30 and ~50–60°2θ. Basing on short-range structural model proposed by Southon et al. [19], reproducible extremely broadened peaks on diffractograms of hydrous zirconia xerogels can be caused by short range ordered zirconium hydroxide polymers consisting of cyclic tetramer species. According to Moroz et al. hydrous zirconia gels precipitated at pH 7 and pH 9 are indeed X-ray amorphous [20] but possess short-range ordering [21]. Amorphous nature of sulphated zirconia xerogels was also confirmed by TEM and SAED patterns of the samples.

According to TGA (Fig. 3A) and TGA–MS (see Fig. S2 in the Supporting Information) data the first stage of thermal decomposition of sulfated zirconia xerogels at temperatures up to approximately 200 °C corresponds to elimination of physisorbed water, and the second one (at 600–750 °C) corresponds to decomposition of sulfates.

Thermal analysis shows that precipitation conditions substantially affect the chemical composition and thermal behavior of sulfated zirconia gels. Weight loss at high temperature decomposition stage decreases notably with the increase in the xerogel precipitation pH. This effect is obviously due to the less content of sulfates in hydrous zirconia samples precipitated at higher pH values and corresponds well to observations made in [22]. These data are also in a good agreement with our recent results on thermal decomposition of non-sulfated hydrous zirconia [7]. It is well known that hydrous oxides generally possess extremely high sorption capacity. Below the point of zero charge (pH_{pzc}) their surface is positively charged and this charge is compensated by preferential adsorption of negatively charged ions. Thus sedimentation of hydrous zirconia under acidic conditions is accompanied by considerable adsorption of NO_3^- and SO_4^{2-} ions which are present in mother liquor. However, higher bonding strength of sulfate ions results in preferred adsorption of SO_4^{2-}. These species cannot be removed completely even by repeated washing.

Temperature corresponding to maximum rate of sulfates decomposition decreases with the increase in the precipitation pH and is equal to 715–725 °C, 685–695 °C, 650–660 °C for Z-4S, Z-7S and Z-9S samples, respectively. This effect is probably caused by the stronger bonding between SO_4^{2-}-ions and hydrous zirconia particles when precipitation is conducted under acidic conditions.

Differential TGA curve of Z-4S sample shown in Fig. 3B exhibits a distinct decomposition stage at 430–500 °C which is absent for the other samples. According to TGA–MS data this stage corresponds to decomposition of nitrate-containing zirconium compounds. Thus, hydrous zirconia precipitated under acidic conditions contains not only high amount of sulfate species, but also a certain amount of NO_3^- ions. Two peaks in the range of 600–750 °C are attributed to two-stage decomposition of sulfate groups. This evidences the presence of at least two types of surface sulfate species.

The body of TGA–MS and differential TGA data gave us the possibility to estimate the chemical composition of sulfated zirconia xerogels: Zr-4S—$ZrO_{1.46}(NO_3)_{0.12}(SO_4)_{0.48} \cdot 2.2H_2O$; Zr-7S—$ZrO_{1.76}(SO_4)_{0.24} \cdot 2.6H_2O$; Zr-9S—$ZrO_{1.88}(SO_4)_{0.12} \cdot 2.7H_2O$. Mass spectroscopy data shows no signal corresponding to sulfur oxides at temperatures below 500–550 °C since SO_4^{2-} groups are chemically bonded to zirconia particles and no other sulfur-containing compounds (like ammonium sulfates or sulfuric acid) are present in samples.

DTA data are presented in Fig. 4. Strong endothermic peak below ~200 °C which is observed for all the samples corresponds to elimination of physisorbed water from zirconia xerogels. At higher temperatures a notable difference in samples behavior is observed. An exothermic peak (maximum at 590–600 °C) for Z-9S sample does not correspond to release of any gaseous products and so it is probably caused by crystallization of zirconia from

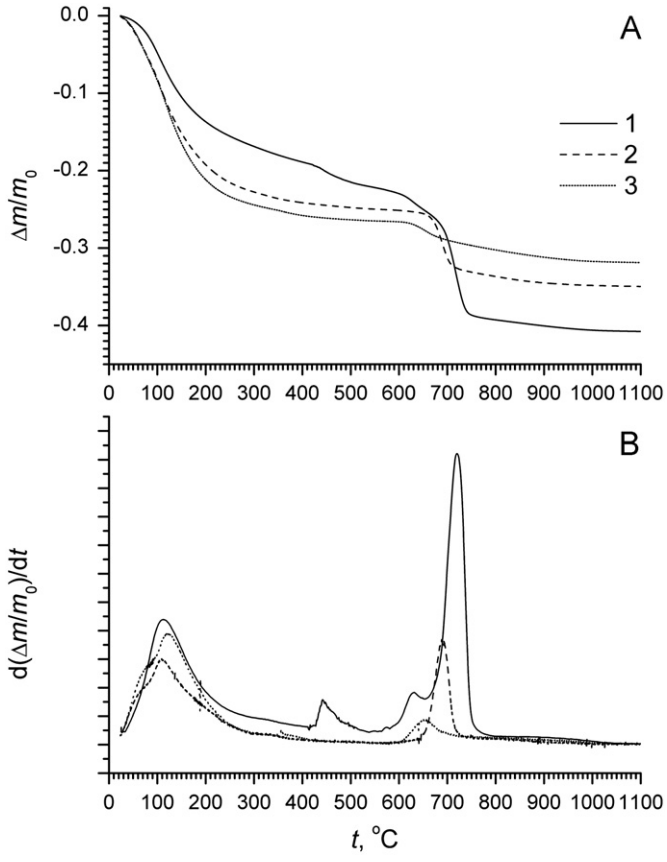

Fig. 3. Thermal analysis (A) and differential thermal analysis (B) curves of sulfated zirconia xerogels precipitated at different pH (1—Z-4S, 2—Z-7S, 3—Z-9S).

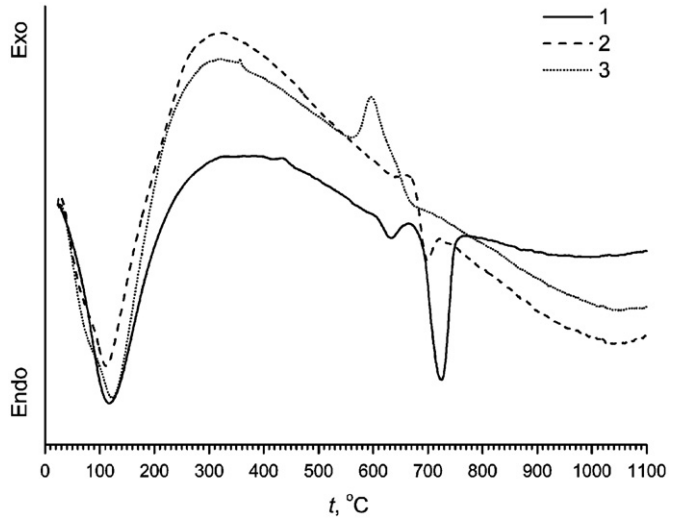

Fig. 4. Differential thermal analysis of sulfated zirconia xerogels (1—Z-4S, 2—Z-7S, 3—Z-9S).

X-ray amorphous state. In turn, non-sulfated zirconia synthesized under the same conditions crystallizes at 415–435 °C. Thus, introduction of sulfate ions favors additional stabilization of amorphous zirconia and inhibits crystallization process. This conclusion is also in line with [22].

DTA curves for Z-7S and Z-4S samples show no evident exothermic effects corresponding to crystallization of ZrO_2. On the contrary, DTA curve for Z-7S sample shows endothermic effect at 700–705 °C which corresponds to decomposition of sulfates, while Zr-4S sample exhibits two close endothermic effects with maxima at 630–635 and 720–725 °C which are also due to the elimination of sulfur oxides. The absence of exothermic crystallization peaks for Z-4S and Z-7S xerogels is probably because of superposition of two opposite sign thermal effects caused by decomposition of sulfates and crystallization of ZrO_2.

Stabilization of amorphous zirconia by sulfate species was confirmed by X-ray diffraction of $ZrO_2 \cdot xH_2O$ samples subjected to long term (5 h) annealing at 500–700 °C (Fig. 5). While Z-9S xerogel which contains minimum amount of sulfates crystallizes upon annealing at 500 °C, Z-4S and Z-7S samples treated under the same conditions remain completely or almost completely amorphous (Z-4S-500 sample contains trace amounts of crystalline zirconia in addition to amorphous phase). Increase in annealing temperature to 550 °C results in notable decrease in the amount of amorphous phase in the samples. Further temperature rise up to 600 °C results in formation of crystalline ZrO_2 in all the

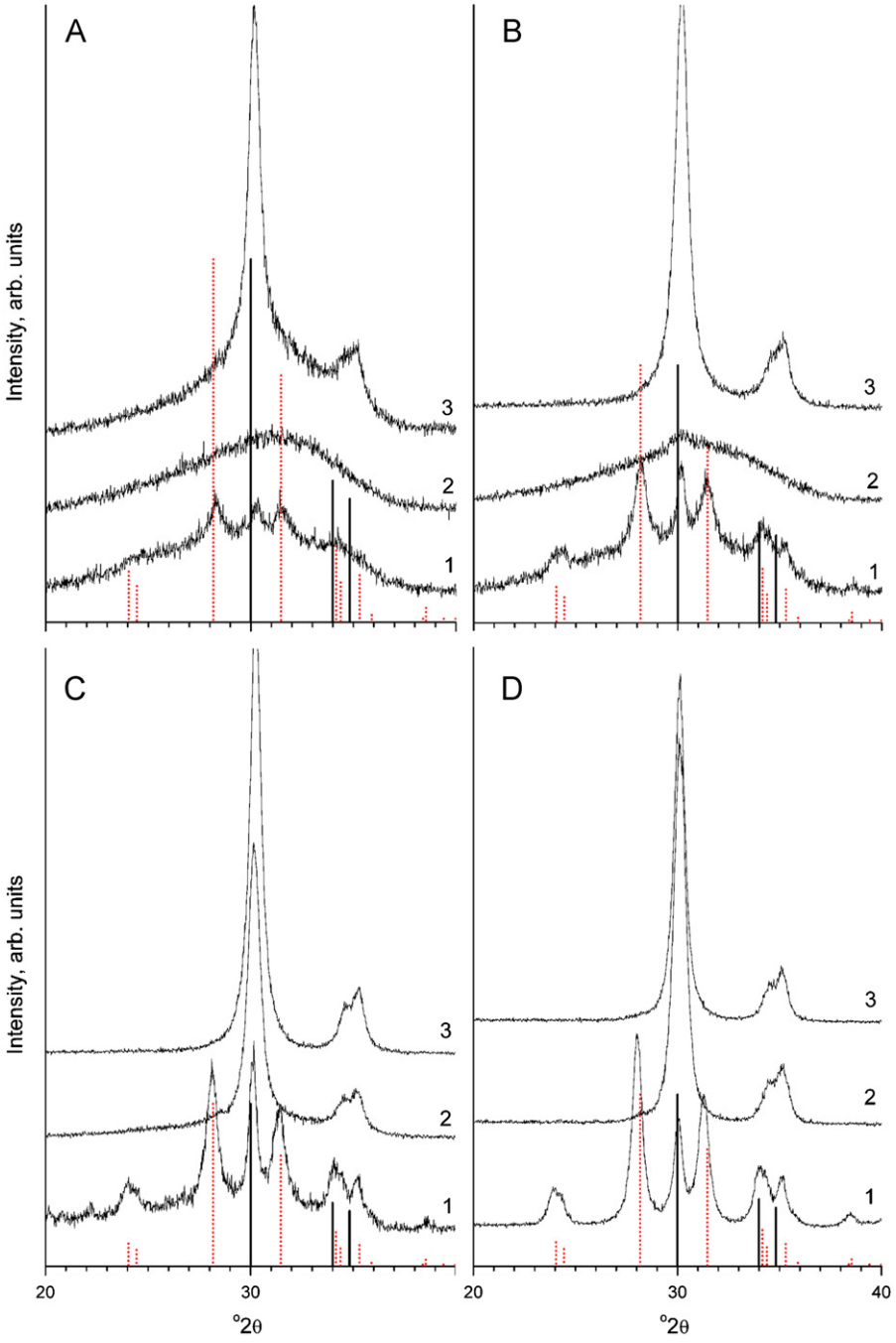

Fig. 5. X-ray diffraction patterns of sulfated zirconia xerogels upon thermal treatment at (a) 500 °C, (b) 550 °C, (c) 600 °C, (d) 700 °C during 5 h (1—pH 4, 2—pH 7, 3—pH 9). Solid black vertical lines correspond to tetragonal zirconia, dotted red ones—to monoclinic zirconia.

cases while small amounts of amorphous zirconia still remain in Z-4-600 and Z-7-600 samples. Complete crystallization occurs only after 5 h treatment at 700 °C.

Phase composition (content of metastable tetragonal and stable monoclinic zirconia) depends on a number of factors including chemical composition of zirconium-containing amorphous precursors. Thermal treatment of Z-7S and Z-9S samples leads to formation of metastable tetragonal zirconia with no marked traces of monoclinic phase. On the contrary, powders obtained upon annealing of Z-4S sample at 500–700 °C contain notable amount of monoclinic zirconia (tetragonal to monoclinic zirconia volume fraction ratio is 1:3–1:4).

Phase composition of sulfated and non-sulfated zirconia obtained under the same conditions differs dramatically. An illustration of this difference is given in Fig. 6 and in Table 4. In non-sulfated samples tetragonal zirconia content decreases with increase in the precipitation pH, while sulfated ones show an opposite tendency.

This result is quite unusual. It is well known that stabilization of tetragonal zirconia is caused by the presence of various anionic and cationic impurities [23]. $ZrO_2 \cdot xH_2O$ precipitated in acid media (below the point of zero charge) indeed contains the highest amount of impurities. Thus products of the thermal decomposition of hydrous zirconia precipitated in acid media in the absence of sulfate species contain higher fraction of tetragonal zirconia in comparison with zirconia precipitated in alkaline media [7]. In turn, to explain unusual behavior of sulfated zirconia we had to take into consideration the second possible stabilization mechanism of tetragonal ZrO_2 described elsewhere [24] which deals with surface excess energy of sub-30 nm zirconia particles.

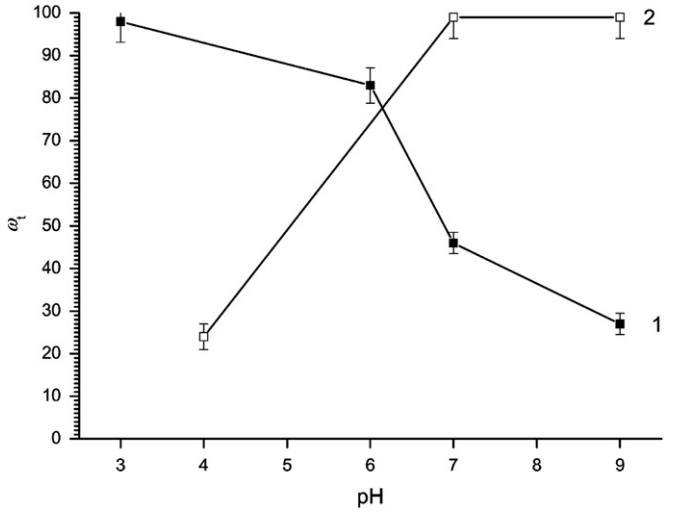

Fig. 6. Relative content of tetragonal zirconia in ZrO_2 samples precipitated at various pH and then annealed at 600 °C for 5 h. 1 – non-sulfated zirconia according to [7], 2 – sulfated zirconia synthesized in this work.

Actually, mean particle size calculated using Scherrer formula notably depends on the precipitation pH. Particle size of tetragonal zirconia obtained upon thermal treatment of sulfated zirconia xerogels precipitated at low pH values (23–28 nm) is notably higher compared with particle size of *t*-ZrO_2 synthesized in neutral and alkaline media (14–16 nm). This effect is in a good accordance with transmission electron microscopy data (Fig. 7). Upon the rise of the temperature from 500 °C to 700 °C the particle size of tetragonal zirconia does not change significantly. The same effect is observed for monoclinic ZrO_2 forming upon thermal decomposition of Z-4S xerogel—particle size of monoclinic ZrO_2 is always about 15–18 nm (see Table 4).

The decrease in particle size of *t*-ZrO_2 with the increase in the precursor xerogels precipitation pH is in line with our previously reported data [7,25]. As far as thermal decomposition of hydrous sulfated zirconia can be judged as a topochemical process, structure of initial xerogel should affect the structure and properties of the product of its thermal decomposition. In particular, xerogel precipitated in acid media has higher apparent density compared to xerogels precipitated in neutral and alkaline media. This was also the case for non-sulfated zirconia. Denser xerogels precipitated at low pH values transform into larger ZrO_2 particles while xerogels possessing more ramified structure decompose upon annealing with formation of relatively small ZrO_2 particles.

Thermal behavior of Z-4S-600, Z-7S-600, and Z-9S-600 samples (Fig. S3 in the Supporting Information) is in line with the above outputs. Weight loss corresponding to elimination of sulfur oxides decreases with increase in the precipitation pH of initial xerogel. Furthermore, the temperature corresponding to the maximum rate of sulfate decomposition falls with the increase in the precipitation pH and is equal to 695–700 °C, 655–665 °C, and 625–635 °C for Z-4S-600, Z-7S-600, and Z-9S-600, respectively.

Chemical composition of xerogels upon annealing at 500 °C and 600 °C according to energy dispersive X-ray spectroscopy data is given in Table 2 and in Table 4. These data also confirm

Table 2
Sulfur content (wt% S) in sulfated zirconia samples.

Precipitation pH	Temperature	
	500 °C	600 °C
3.98	8.1	7.7
6.98	8.5	5.0
8.98	4.7	2.8

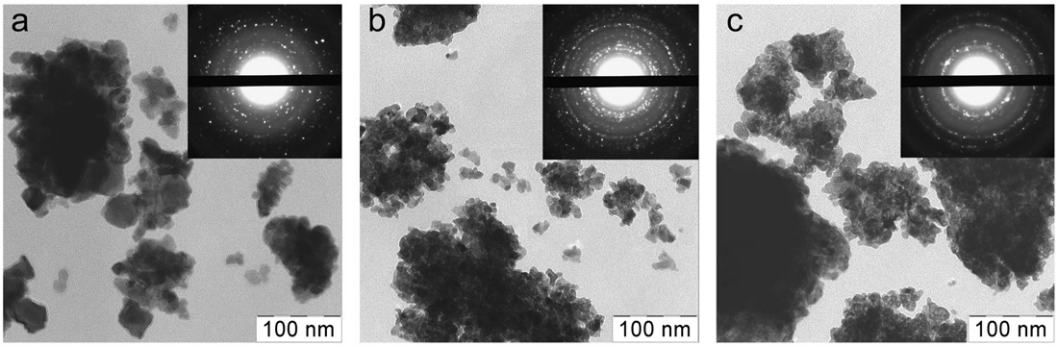

Fig. 7. TEM images of sulfated zirconia samples Z-4S-600 (a), Z-7S-600 (b), Z-9S-600 (c).

that sulfur content in sulfated nanocrystalline zirconia decreases with the rise of hydrous zirconia precipitation pH and agree with the thermal analysis data presented in Fig. 3 and S3. Temperature rise from 500 °C to 600 °C does not substantially affect the sulfur content in powders derived from Z-4S, while lead to 1.5 and 2.0-fold decrease in sulfur content in ZrO_2 powders derived from Z-7S and Z-9S samples, respectively. This is in a good agreement with the above conclusion that raise in the precipitation pH facilitates sulfates decomposition and lowers the temperature of sulfur oxides elimination.

Specific surface area values of Z-4S, Z-7S, and Z-9S xerogels treated at 500 °C, 550 °C, and 600 °C are given in Fig. 8 and in Table 4. Specific surface area rises with the increase in the precipitation pH as well as with the raise of the temperature of thermal treatment. Close results on the influence of pH on the amount of sulfate sorbed as well as effect of calcination temperature on surface area of sulfated zirconia was reported earlier by [26]. Actually specific surface area (S_{BET}) of samples originated from Z-4S xerogel is very low and do not exceed 20 m^2/g. At the same time increase in the precipitation pH up to the point of zero charge and higher leads to dramatic increase in corresponding specific surface area values. These data give additional evidence that initial amorphous hydrous zirconia mesostructure influences the microstructure of nanocrystalline sulfated zirconia. The highest surface area of zirconia can be reached when starting hydrous zirconia is precipitated under alkaline conditions ($pH > pH_{pzc}$). These data correlates well with the Arata's pioneering work [26]. Increase in specific surface area values with the raise of annealing temperature is presumably caused by elimination of gaseous products from sulfated zirconia causing formation of microcracks. SEM images (see Fig. 9) support surface area measurements and vividly present the difference between dense glass-like structure of Z-4S-600 sample and porous structure of Z-7S-600 and Z-9S-600 samples.

Table 3
Catalytic isomerization and oligomerization of hexene-1 over sulfated zirconia.

Run	Catalyst	t, °C/τ, h	Conversion, %	Products content, %				
				C_6	C_{12}	C_{18}	C_{24}	C_{30}
1	Z-4S-600	20/1	6					
2		20/24	54					
3		40/1	60					
4		60/1	67	78[a]	16	6	0	0
5	Z-7S-600	20/1	58					
6		20/24	100					
7		40/1	100	18[b]	49	24	7	2
8		60/1	100					
9	Z-9S-600	20/1	74					
10		20/24	100					
11		40/1	100	13[b]	45	26	10	4
12		60/1	100					

[a] ~30% of hexene-1.
[b] Only hexene-2+hexene-3.

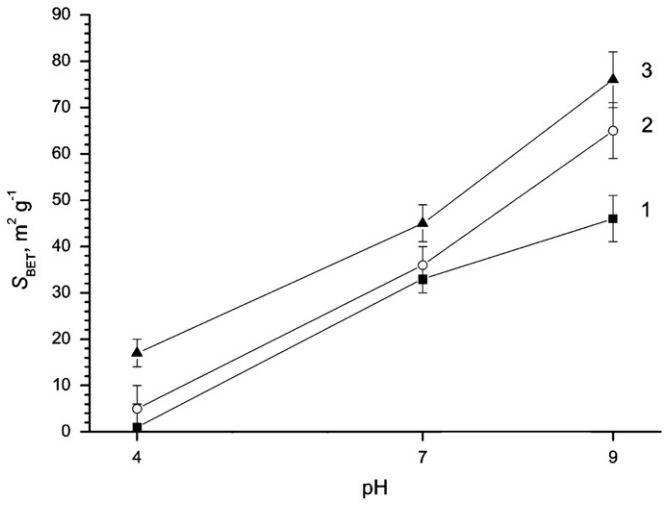

Fig. 8. Specific surface area of sulfated zirconia against precipitation pH and temperature of thermal treatment (1–500 °C, 2–550 °C, 3–600 °C).

Fig. 10 represents NH_3 temperature-programmed desorption (TPD) spectra normalized per 1 m^2 surface area for sulfated zirconia samples annealed at 600 °C for 5 h. The surface of all samples contains acid sites of two different types. Low temperature peaks at 150–200 °C in NH_3-TPD spectra correspond to weak acid centers. Extended shoulders with no pronounced maxima which appear at 250–600 °C correspond to strong acid sites. Increase in initial xerogel precipitation pH leads to the raise of the ratio between weak and strong acid centers. As weak acid sites are commonly assigned to the surface hydroxyl groups, the surface of sulfated zirconia remains hydroxylated even upon annealing at 600 °C. Distribution of weak acid sites over ammonium desorption activation energy becomes narrower in a row of Z-4S-600, Z-7S-600, and Z-9S-600. This can be explained by higher phase uniformity of samples obtained upon annealing of xerogels precipitated at higher pH (see Fig. 5c). Note that Z-4S-600 sample possesses the highest concentration of strong acid sites. When adsorbed on oxide surfaces sulfate species generate strong acidity [3,4] through both Lewis and Brønsted superacid centers [2]. Accordingly sulfated zirconia synthesized from xerogel precipitated at the lowest pH possess the highest sulfur to zirconium molar ratio.

Surface concentration of acid sites can be determined by integrating the NH_3-TPD curves, supposing that each NH_3 molecule desorbs from one site. Z-4S-600 sample showed the highest specific concentration of acid sites (18.6 μmol/m^2), while the values for Z-7S-600 and Z-9S-600 are quite close and are equal to 6.5 and 8.9 μmol/m^2, respectively (see Table 4).

To estimate the catalytic activity of sulfated zirconia we have studied hexene-1 oligomerization catalyzed by Z-4S-600, Z-7S-600, and Z-9S-600 samples. During each experiment a portion of pure hexene-1 was stirred with a catalyst at a predetermined temperature. Analysis of reaction mixtures was performed by ^1H NMR and GC–MS methods. The catalytic transformation of

Table 4
Properties of sulfated zirconia catalysts.

Sample	Surface area, m^2/g	Particle size (XRD), nm		Volume fraction of t-ZrO_2, %	Sulfur content, wt%	Specific acidity, μmol/m^2	Total acidity, μmol/g	Conversion of hexene-1 at 40/1 run (see Table 3), %
		t-ZrO_2	m-ZrO_2					
Z-4S-600	17 ± 3	26 ± 2	17 ± 2	24 ± 3	7.7 ± 0.4	18.6 ± 0.6	320 ± 50	60 ± 3
Z-7S-600	45 ± 4	15 ± 1	–	100	5.0 ± 0.3	6.4 ± 0.4	290 ± 50	100
Z-9S-600	76 ± 6	16 ± 1	–	100	2.8 ± 0.3	8.9 ± 0.4	680 ± 50	100

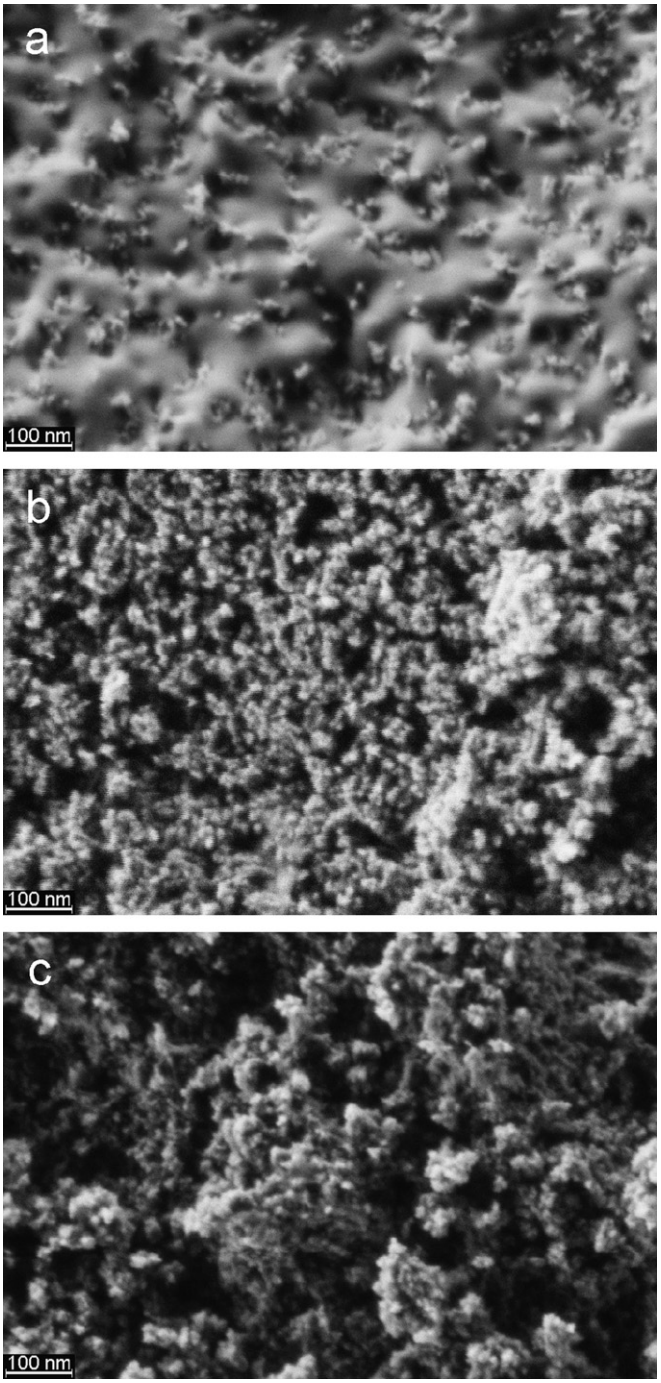

Fig. 9. SEM images of Z-4S-600 (a), Z-7S-600 (b), and Z-9S-600 (c) samples.

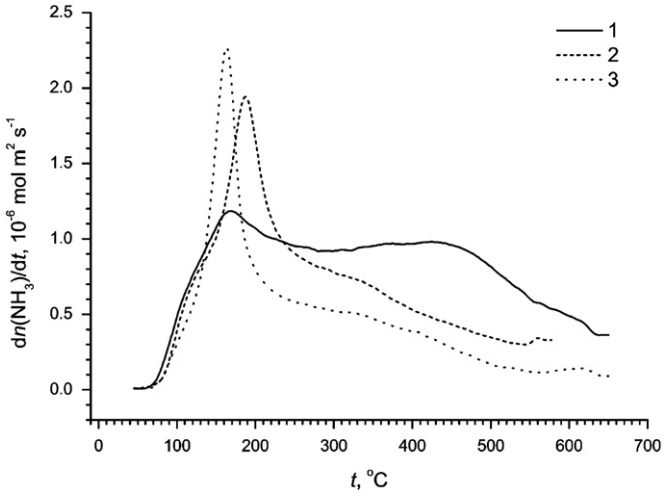

Fig. 10. NH_3-TPD data normalized per 1 m^2 of surface area of sulfated zirconia (1—Z-4S-600, 2—Z-7S-600, 3—Z-9S-600).

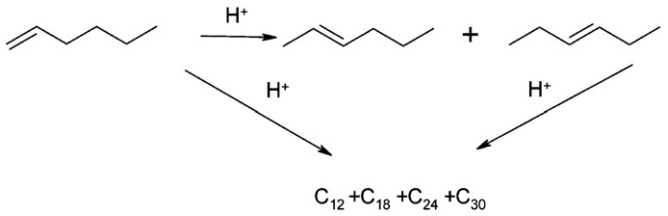

Scheme 1. Chemical transformations catalyzed by sulfated zirconia. .

hexene-1 under acid conditions leads to a double bond shift and/or to oligomerization resulting in formation of higher olefins. Catalytic reaction scheme is given in Scheme 1 and the results are summarized in Tables 3 and 4. The influence of precipitation pH on the catalytic activity of sulfated zirconia in oligomerization as well as on side isomerisation reaction of hexene-1 can be easily observed. The data obtained correlate well with earlier short communication of Arata et al. devoted to catalytic isomerization of *n*-pentane [27].

Table 4 summarizes properties of sulfated zirconia catalysts.

The results of catalytic experiments can be explained from the point of view of surface acidic properties of the samples (see Table 4). Z-4S-600 sample has the highest specific acidity (18.6 μmol/m^2) but the lowest specific surface area (17 m^2/g), what gives the value of total acidity approx. 320 μmol/g. The Z-9S-600 sample with 8.9 μmol/m^2 specific acidity and 76 m^2/g surface area gives more than a two times higher total acidity value—approx. 680 μmol/g. This means that 1 g of Z-9S-600 catalyst will be at least two times more active in catalytic transformation of hexene-1 than an equivalent amount of Z-4S-600 catalyst. The difference in catalytic activity must be even larger because of the surface structure of the samples—glass-like for Z-4S-600 and porous for Z-9S-600 (Fig. 9). The total acidity of Z-7S-600 sample (approx. 290 μmol/g) is close to Z-4S-600, but the porous surface structure makes it more active.

4. Conclusions

In this work, we have established how mesostructure and composition of hydrous sulfated zirconia gels precipitated from $ZrO(NO_3)_2/(NH_4)_2SO_4$ aqueous solutions at different pHs govern structure, chemical and phase composition, and catalytic activity of nanocrystalline sulfated zirconia formed *via* thermal decomposition of these gels. We have shown for the first time that the raise in precipitation pH from 4 to 9 leads to dramatic increase in the surface fractal dimension (D_S) of sulfated zirconia xerogels as well as to a decrease in the size of primary particles (r_c) forming zirconia fractal aggregates. Sulfated nanocrystalline zirconia samples prepared from gels precipitated in neutral and alkaline media have relatively low sulfur content but they possess much higher catalytic activity due to the smaller particle size, higher specific surface area and higher total acidity. We hope this paper makes a contribution to reproducible synthetic methods of sulfated zirconia superacid catalysts preparation.

Acknowledgments

Authors are grateful to Dr. Tatyana I. Vetrova for technical assistance.

V.I., A.B. and G.K. would like to thank GKSS Forschungszentrum for hearty welcome.

The work was partially supported by the Russian Ministry of Science and Education (project ♯14.740.11.0281) and Russian Foundation for Basic Research (projects 09-03-01067 and 11-03-00981).

Appendix A. Supporting information

Supplementary data associated with this article can be found in the online version at http://dx.doi.org/10.1016/j.jssc.2012.11.022.

References

[1] Y. Wu, S. Liao, Front. Chem. Eng. Chin. 3 (2009) 330.
[2] J.R. Sohn, J. Ind. Eng. Chem. 10 (2004) 1.
[3] M. Waqif, J. Bachelier, O. Saur, J.C. Lavalley, J. Mol. Catal. 72 (1992) 127;
B.M. Reddy, M.K. Patil, Chem. Rev. 109 (2009) 2186;
K. Arata, Green Chem. 11 (2009) 1719;
S.G. Ryu, B.C. Gates, Ind. Eng. Chem. Res. 37 (1998) 1786;
S. Rezgui, R.E. Jentoft, B.C. Gates, Catal. Lett. 51 (1998) 229;
T.K. Cheung, F.C. Lange, B.C. Gates, J. Catal. 159 (1996) 99.
[4] K. Arata, H. Matsushita, M. Hino, H. Nakamura, Catal. Today 81 (2003) 17.
[5] H. Yu, H. Fang, H. Zhang, B. Li, F. Deng, Catal. Commun. 10 (2009) 920.
[6] M.K. Mishra, B. Tyagi, R.V. Jasra, Ind. Eng. Chem. Res. 42 (2003) 5727;
S. Wrabets, X. Yang, G. Tzolova-Müller, R. Schlögl, F.C. Jentoft, J. Catal. 269 (2010) 351;
A. Minesso, F. Genna, T. Finotto, A. Baldan, A. Benedetti, J. Sol–Gel Sci. Techn. 24 (2002) 197;
C.-Y. Hsu, C.R. Heimbuch, C.T. Armes, B.C. Gates, J. Chem. Soc., Chem. Commun. (1992) 1645;
Z. Yanwei, Z. Yubao, J. Colloid Interface Sci. 247 (2002) 100;
B.M. Reddy, P.M. Sreekanth, P. Lakshmanan, A. Khan, J. Mol. Catal. A 244 (2006) 1;
S. Ardizzone, C.L. Bianchi, E. Grassi, Colloids Surf. 135 (1998) 41;
H.K. Mishra, K.M. Parida, Appl. Catal., A 224 (2002) 179.
[7] V.K. Ivanov, G.P. Kopitsa, A.E. Baranchikov, M. Sharp, K. Pranzas, S.V. Grigoriev, Russ. J. Inorg. Chem. 54 (2009) 2091.
[8] H. Toraya, M. Yoshimura, S. Somiya, J. Am. Ceram. Soc. 67 (1984) C–119.
[9] G.D. Wignall, F.S. Bates, J. Appl. Crystallogr. 20 (1986) 28.
[10] W. Schmatz, T. Springer, J. Schelten, K. Ibel, J. Appl. Crystallogr. 7 (1974) 96.
[11] H.D. Bale, P.W. Schmidt, Phys. Rev. Lett. 38 (1984) 596.
[12] P.W. Schmidt, Modern Aspects of Small-Angle Scattering, Kluwer Academic Publishers, Dordrecht, 1995.
[13] G.P. Kopitsa, V.K. Ivanov, S.V. Grigoriev, P.E. Meskin, O.S. Polezhaeva, V.M. Haramus, JETP Lett. 85 (2007) 122.
[14] G. Beaucage, J. Appl. Crystallogr. 28 (1995) 717.
[15] A. Guinier, G. Frournet, C.B. Walker, K.L. Yudowitch, Small-Angle Scattering of X-rays, Wiley, New York, 1955.
[16] C.J. Brinker, K.D. Keefer, D.W. Schaeffer, R.A.Q. Assink, B.D. Kay, C.S. Ashley, J. Non-Cryst. Solids 63 (1984) 45.
[17] A. Clearfield, J. Mater. Res. 5 (1990) 161.
[18] T.G. Kuznetsova, V.A. Sadykov, Kinet. Catal. 49 (2008) 840.
[19] P.D. Southon, J.R. Bartlett, J.L. Woolfrey, B. Ben-Nissan, Chem. Mater. 14 (2002) 4313.
[20] D.A. Zyuzin, E.M. Moroz, A.S. Ivanova, A.N. Shmakov, G.N. Kustova, Kinet. Catal. 45 (2004) 739.
[21] D.A. Zyuzin, E.M. Moroz, A.S. Ivanova, A.N. Shmakov, Crystallogr. Rep. 48 (2003) 413.
[22] S. Chokkaram, R. Srinivasan, D.R. Milburn, B.H. Davis, J. Colloid Interface Sci. 165 (1994) 160.
[23] S. Shukla, S. Seal, Int. Mater. Rev. 50 (2005) 1.
[24] R.C. Garvie, J. Phys. Chem. 69 (1965) 1238;
E. Djurado, P. Bouvier, G. Lucazeau, J. Solid State Chem. 149 (2000) 399;
S. Shukla, S. Seal, R. Vij, S. Bandyopadhyay, Z. Rahman, Nano Lett. 2 (2002) 989;
S. Shukla, S. Seal, J. Phys. Chem. B 108 (2004) 3395;
S. Shukla, S. Seal, Rev. Adv. Mater. Sci. 5 (2003) 117.
[25] V.K. Ivanov, G.P. Kopitsa, A.E. Baranchikov, S.V. Grigor'ev, V.M. Haramus, Russ. J. Inorg. Chem. 55 (2010) 155.
[26] F.R. Chen, G. Coudurier, J.F. Joly, J.C. Vedrine, J. Catal. 143 (1993) 616;
A. Corma, A. Martínez, C. Martínez, Appl. Catal., A 144 (1996) 249.
[27] T. Tatsumi, H. Matsuhashi, K. Arata, Bull. Chem. Soc. Jpn. 69 (1996) 1191.